a Waters Radial Pak silica column and an 80/20 hexane/chloroform (Aldrich, ethanol stabilized) mixture as eluent.

Acknowledgment. We acknowledge the National Science Foundation (Grants CHE83-01776 and CHE85-17632) for financial support of this work. Dr. Jerry Liu is thanked for several helpful discussions concerning the synthesis of CAB.

Registry No. CAB, 105900-20-7; CAB dimer, 105900-21-8; 2-methoxyanthracene, 42298-28-2; phthalic anhydride, 85-44-9; anisole, 100-66-3; 2-hydroxyanthracene, 613-14-9; ethyl 4-(2-anthryloxy)butanoate, 105930-59-4; ethyl 4-bromobutanoate, 2969-81-5; 4-(2-anthryloxy)butanoic acid, 105930-60-7; 4-(2-anthryloxy)butanoyl chloride, 105930-61-8; cholesterol, 57-88-5.

References and Notes

(1) This paper is part 24 in our series "Liquid-Crystalline Solvents as Mechanistic Probes". For part 23, see: Treanor, R. L.; Weiss, R. G. *Tetrahedron*, in press.
(2) Lin, Y.-c.; Weiss, R. G., unpublished results.
(3) See for instance: (a) Hermans, P. H. In *Colloid Science. Reversible Systems*; Kruyt, H. R., Ed.; Elsevier: Amsterdam, 1969; Vol. II, Chapter XII. (b) Flory, P. J. *Discuss. Faraday Soc.* **1974**, *57*, 7.
(4) (a) Terech, P.; Volino, F.; Ramasseul, R. *J. Phys. (Paris)* **1985**, *46*, 895. (b) Terech, P. *J. Colloid Interface Sci.* **1985**, *107*, 244. (c) Ramasseul, R.; Rassat, A. *Tetrahedron Lett.* **1974**, 2413.
(5) Campbell, J.; Kuzma, M.; Labes, M. M. *Mol. Cryst. Liq. Cryst.* **1983**, *95*, 45.
(6) Yoshioka, H.; Honda, K.; Kondo, M. *J. Colloid Interface Sci.* **1983**, *93*, 540.
(7) Wilkens, L. S.; Reid, R. C. *J. Colloid Interface Sci.* **1981**, *79*, 535.
(8) Hidaka, H.; Murata, M.; Onai, T. *J. Chem. Soc., Chem. Commun.* **1984**, 562.
(9) Tachibana, T.; Mori, T.; Hori, K. *Bull. Chem. Soc. Jpn.* **1980**, *53*, 1714.
(10) Vaterrodt, P. U.S. Patent2 719 782, Oct 4, 1955.
(11) Weissberger, A.; Leiserson, J. L. U.S. Patent 2 388 887, May 6, 1946.
(12) Hill, P.; Van Strien, R. E. U.S. Patent 2 751 284, June 19, 1956.
(13) Saito, T.; Matsuzawa, Y.; Ninagawa, S.; Honna, M.; Takesada, M.; Takehara, M. U.S. Patent 3 969 087, July 13, 1976.
(14) (a) Twieg, R. J.; Russell, T. P.; Siemens, R.; Rabolt, J. R. *Macromolecules* **1985**, *18*, 361. (b) Mahler, W., private communication.
(15) Birks, J. B. *Photophysics of Aromatic Molecules*; Wiley-Interscience: London, 1970; Chapter 7.
(16) (a) Novak, T. J.; Mackay, R. A.; Poziomek, E. J. *Mol. Cryst. Liq. Cryst.* **1973**, *20*, 213. (b) Anderson, V. C.; Craig, B. B.; Weiss, R. G. *J. Am. Chem. Soc.* **1981**, *103*, 7169.
(17) Weinberger, R.; Cline Love, L. J. *Spectrochim. Acta, Part A* **1984**, *40a*, 49.
(18) (a) Mason, S. F.; Peacock, R. D. *Chem. Phys. Lett.* **1973**, *21*, 406. (b) Platt, J. R. *J. Chem. Phys.* **1949**, *17*, 484.
(19) (a) Chandross, E. A. *J. Chem. Phys.* **1965**, *43*, 4175. (b) Ferguson, J.; Mau, A. W. H.; Morris, J. M. *Aust. J. Chem.* **1973**, *26*, 91, 103. (c) Chandross, E. A.; Ferguson, J.; McRae, E. G. *J. Chem. Phys.* **1966**, *45*, 3546. (d) Chandross, E. A.; Ferguson, J. *Ibid.* **1966**, *45*, 3554. (e) Martinaud, M. These de Docteur d'Etat Es-Sciences, University of Bordeaux I, Talence, France, 1975. (f) Martinaud, M.; Kottis, Ph. *J. Phys. Chem.* **1978**, *82*, 1497.
(20) See, for instance: Anderson, V. C.; Weiss, R. G. *J. Am. Chem. Soc.* **1984**, *106*, 6628.
(21) (a) Saeva, F. D. *Pure Appl. Chem.* **1974**, *38*, 25 and references cited therein. (b) Saeva, F. D. In *Liquid Crystals. The Fourth State of Matter*; Saeva, F. D., Ed.; Marcel-Dekker: New York, 1979; Chapter 6.
(22) Angles from 3° to 30° were scanned on a Picker diffractometer using Mo Kα (λ = 0.7107 Å) radiation. We thank Dr. Geoffrey B. Jameson for his assistance with these experiments.
(23) Demus, D.; Richter, L. *Textures of Liquid Crystals*; Verlag Chemie: Weinheim, 1978.
(24) (a) Ferguson, J.; Mau, A. W. H. *Mol. Phys.* **1974**, *27*, 377. (b) Marcondes, M. E. R.; Toscano, V. G.; Weiss, R. G. *J. Am. Chem. Soc.* **1975**, *97*, 4485.
(25) (a) Iwata, M.; Emoto, S. *Bull. Chem. Soc. Jpn.* **1974**, *47*, 1687. (b) Fieser, L. F.; Williamson, K. L. *Organic Experiments*, 3rd ed.; D. C. Heath: Lexington, MA, 1975; p 240.
(26) McOmie, J. F. W.; Watts, M. L.; West, D. E. *Tetrahedron* **1968**, *24*, 2289.

Dual-Mode Transport of Molecular Oxygen in a Membrane Containing a Cobalt Porphyrin Complex as a Fixed Carrier

Hiroyuki Nishide, Manshi Ohyanagi, Osamu Okada, and Eishun Tsuchida*

Department of Polymer Chemistry, Waseda University, Tokyo 160, Japan.
Received May 5, 1986

ABSTRACT: Molecular oxygen transport through a polymeric membrane is found to be augmented by the addition of [$\alpha,\alpha',\alpha'',\alpha'''$-*meso*-tetrakis(*o*-pivalamidophenyl)porphinato]cobalt(II)–1-methylimidazole (CoPIm) complex, which forms an oxygen adduct rapidly and reversibly. The oxygen-binding rate and equilibrium constants for the Co complex in the membrane, i.e., a fixed carrier, were measured spectroscopically in situ. The oxygen permeability of the membrane containing CoPIm increased with decreasing upstream oxygen pressure, which is in accordance with a dual-mode transport model. The oxygen-binding parameters, determined spectroscopically, were adequate for an approximate analysis in terms of this model. The permeability ratio (P_{O_2}/P_{N_2}) was greater than 10 in the membrane containing a large amount of CoPIm.

Introduction

Much effort has been expended in studying the selective transport of gases through polymeric membranes.[1] One method that has been reported to find oxygen permselective membrane is the syntheses of polymers in which the solubility coefficient of oxygen is greater than that of nitrogen.[2,3] However, it is difficult to prepare a polymer in which only the oxygen solubility coefficient is substantially enhanced. This is easily understood from the fact that there is only a small difference between the solubilities of oxygen and nitrogen in organic solvents. In fact, no permselective membrane has been successfully prepared by this approach.

A polymer containing a carrier that interacts specifically and reversibly with oxygen would be an interesting possibility as an oxygen permselective membrane. Metal complexes such as iron porphyrin derivatives and cobalt–Schiff base complexes form oxygen adducts reversibly and bind oxygen according to a Langmuir isotherm. This approach has been successfully applied as an oxygen-transporting fluid[4] and as oxygen-separating liquid membranes.[5] Oxygen exhibited a high permeability in the latter. However, for the liquid membrane the membrane itself cannot be used under a differential gas pressure, and the liquid medium containing the metal complex is vaporized in use. Thus, it is not feasible to employ an oxygen-enriching membrane to separate oxygen from air.

We preliminarily reported the preparation of a polymer membrane containing a cobalt porphyrin complex as a fixed carrier in the membrane that sorbs and transports

0024-9297/87/2220-0417$01.50/0

oxygen selectively in the Langmuir mode.[6] Oxygen permeation in a membrane containing a cobalt complex using cobalt–Schiff base complexes was also recently reported.[7] The present paper describes highly selective transport of molecular oxygen in a polymer containing a cobalt porphyrin complex as a fixed carrier. We also discuss the permeation profile based on a dual-mode transport model. The polymer membrane was prepared by homogeneously dispersing in poly(butyl methacrylate) the [$\alpha,\alpha',\alpha'',\alpha'''$-*meso*-tetrakis(*o*-pivalamidophenyl)porphinato]cobalt(II)-1-methylimidazole (CoPIm) complex, whose sixth coordination site is vacant even in the solid state and able to bind oxygen reversibly. Rapid and reversible oxygen binding to the complex (the fixed carrier) in the membrane was characterized in situ by spectroscopic methods. The oxygen permeation behavior through the membranes is quantitatively discussed in terms of the combination of dual-mode-transport theory and the spectroscopic data.

Experimental Section

Materials. [$\alpha,\alpha',\alpha'',\alpha'''$-*meso*-tetrakis(*o*-pivalamidophenyl)-porphinato]cobalt(II) (CoP) was synthesized as in the literature.[8] CoP was complexed with 1-methylimidazole (Im) in toluene under a nitrogen atmosphere. Toluene solutions of the CoPIm complex and poly(butyl methacrylate) (PBMA) (M_w = 32 000) were mixed, and the mixed toluene solution was carefully cast on a Teflon plate under an oxygen-free atmosphere, followed by drying in vacuo, to yield a transparent, wine-red membrane with a thickness of 60–65 μm and containing 2.5–4.5 wt % CoPIm.

Spectroscopic Measurements. Reversible oxygen binding to the CoPIm complex in the membrane was observed to be accompanied by a spectral change in the visible absorption (using high-sensitivity spectrophotometer, Shimazu Model UV2000). Rapid and reversible oxygen binding to the CoPIm complex in the membrane was also confirmed by flash photolysis (using a pulse and laser flash spectrophotometer equipped with a kinetic data processor, UNISOKU Model FR-2000). The laser flash was applied perpendicularly to the light path of the spectrophotometer, and the membrane was placed at the crossing of the laser flash and the light path and at 45° to both. The rapid absorption change was recorded with a contact-type photomultiplier to cancel the noise caused by scattered light.

Permeation Measurement. Oxygen permeation coefficients for various upstream gas pressures were measured with a low-vacuum permeation apparatus in the chamber with stable thermostating (Rika Seiki Inc. Model K-315 N-03). The pressure on the upstream side was maintained essentially constant. The pressures on the upstream and downstream sides were detected by using a Baratron absolute pressure gauge (MKS Instruments Inc.). Nitrogen permeation coefficients were measured by the same procedure as for oxygen. The permeation coefficient was calculated from the slope of the steady-state straight line of the permeation curve.

Transport in a Fixed Carrier Membrane

The membrane containing the CoPIm complex as a fixed carrier is assumed to sorb molecular oxygen by a dual mode: Henry's law sorption to the polymer domain and additional Langmuir sorption to the complex. Oxygen adsorption and desorption to the CoPIm complex in solution are known to be very rapid and reversible. If the CoPIm complex is fixed in the membrane with preservation of its oxygen-binding ability, oxygen interacts with the fixed CoPIm carrier rapidly and reversibly and is not immobilized by it during the passage through the membrane. Thus oxygen transport is expected to be accelerated by the additional Langmuir mode in addition to the Henry mode.

Paul and Koros have reported carbon dioxide transport via a frozen free volume or microvoid that arises from the nonequilibrium nature of glassy polymers and proposed a dual-mode-transport theory to explain the behavior of carbon dioxide transport in glassy polymers.[9]

Scheme I

Oxygen Transport System in a Fixed Carrier Membrane

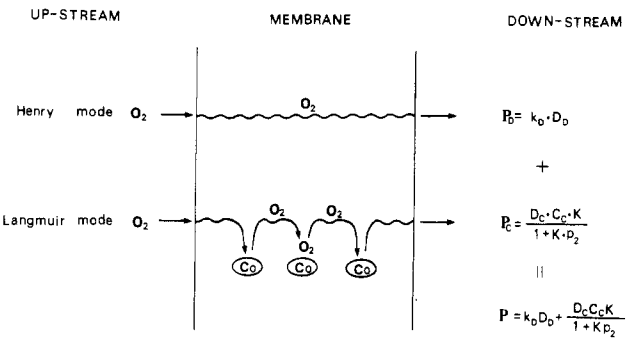

This dual-mode-transport theory is applicable to oxygen transport in the membrane containing the CoPIm complex as a fixed carrier, as mentioned below. Scheme I shows the oxygen permeability in the fixed carrier membrane that is governed by both the Henry and the Langmuir modes. That is, the oxygen permeation coefficient is equal to the sum of a first term representing the Henry mode and a second term representing the Langmuir mode (eq 1).

$$P = k_D D_D + D_C C_C' K/(1 + K p_2) \quad (1)$$

Here, P is the permeability coefficient, k_D is the solubility coefficient for Henry's law, D_D and D_C are the diffusion coefficients for Henry-type and Langmuir-type diffusion, respectively, C_C' is the saturated amount of oxygen reversibly bound to the binding site or fixed carrier, K is the oxygen-binding and dissociation equilibrium constant, and p_2 is the upstream gas pressure. Equation 1 is a function of p_2, and P increases with decreasing p_2.

The time course of the permeation of gas molecules through membranes often shows an induction period followed by permeation with a constant slope (steady state). For a fixed carrier membrane the induction period is expected to be enhanced because the fixed carrier interacts with the penetrant and reduces its diffusivity in the membrane. The induction period for the membrane containing the CoPIm complex is also governed by both the Henry and Langmuir modes (eq 2).[9a]

$$6D_D\theta/l^2 = [1 + R[f_0(y) + FRf_1(y) + (FR)^2 f_2(y)] + FRf_3(y) + (FR)^2 f_4(y)]/[1 + FR/(1 + y)]^3 \quad (2)$$

$$f_0(y) = \frac{6}{y^3}\left[\frac{y^2}{2} + y - (1 + y)\ln(1 + y)\right]$$

$$f_1(y) = \frac{6}{y^3}\left[\frac{y}{2} - \frac{3y}{2(1 + y)} + \frac{\ln(1 + y)}{(1 + y)}\right]$$

$$f_2(y) = \frac{6}{y^3}\left[\frac{1}{6} - \frac{1}{2(1 + y)} + \frac{1}{2(1 + y)^2} - \frac{1}{6(1 + y)^3}\right]$$

$$f_3(y) = \frac{6}{y^3}\left[-\frac{3}{2}y + \frac{y}{2(1 + y)} + (1 + y)\ln(1 + y)\right]$$

$$f_4(y) = \frac{6}{y^3}\left[\frac{1}{2} - \frac{1}{2(1 + y)^2} - \frac{\ln(1 + y)}{(1 + y)}\right]$$

Here, θ is the permeation time lag, F is defined as D_C/D_D, and R is defined as KC_C'/k_D. θ also depends on p_2. Equation 2 is converted into eq 3, where $F = D_C/D_D$, R

$$\frac{6\theta[1 + FR/(1 + y)]^3}{[f_0(y) + FRf_1(y) + (FR)^2f_2(y)]l^2}(Y) = \frac{R}{D_D} + \frac{1 + FRf_3(y) + (FR)^2f_4(y)}{f_0(y) + FRf_1(y) + (FR)^2f_2(y)}(X)\frac{1}{D_D} \quad (3)$$

$= C_C'K/k_D$, $y = Kp_2$, and l is the thickness of the membrane. The combination of eq 3 and 1 gives R/D_D and $1/D_D$, and the permeation parameters, D_C, k_D, and C_C', can be estimated.

Results and Discussion

Oxygen Binding to the Complex in the Membrane. The visible absorption spectrum of the red and transparent membranes is shown in Figure 1. The spectrum of the deoxy CoPIm complex (λ_{max} = 528 nm) was changed to the spectrum with λ_{max} = 545 nm assigned to the oxy CoPIm complex (O_2/Co = 1/1 adduct) immediately after exposure to oxygen. The oxy–deoxy spectral change was reversible in response to a partial pressure of oxygen with isosbestic points at 480, 538, and 667 nm. These visible absorption spectra agreed with those for the corresponding complex in toluene solution.

The reversible oxy–deoxy spectral change occurred very rapidly; e.g., for a 65-μm-thick membrane containing 2.5 wt % CoPIm the oxygen-binding and dissociation equilibrium was established within a few minutes after exposure to oxygen or in vacuo at 25 °C (Figure 2). Although there have been a few reports on oxygen binding to the cobalt–Schiff base complexes or iron porphyrin complexes dispersed in or bonded to polymers in the solid state, oxygen adsorption and desorption on these polymers occurred very slowly even in a finely powdered state with a large surface area.[10] It is important for a fixed carrier of oxygen that oxygen be sorbed and desorbed rapidly in response to a partial oxygen pressure even after fixation in the membrane.

$$\text{CoPIm–O}_2 \xrightarrow{h\nu} \text{CoPIm} + \text{O}_2 \xrightarrow{k_{app}} \text{CoPIm–O}_2 \quad (4)$$

$$\text{CoPIm} + \text{O}_2 \underset{k_{off}}{\overset{k_{on}}{\rightleftharpoons}} \text{CoPIm–O}_2 \quad (5)$$

Photodissociation and recombination of the bound oxygen from and to the CoPIm complex in the membrane (eq 4) was successfully observed by pulse and laser flash spectroscopy. The oxygen-binding and dissociation rate constants (k_{on} and k_{off} in eq 5) of the CoPIm complex fixed in the membrane could be determined in situ as follows. Changing the monitoring wavelength from 510 to 560 nm allowed a differential spectrum before and after flash photolysis to be measured. The positive and negative extremes in the differential spectrum, 528 and 545 nm, were selected as the monitoring wavelengths thereafter (Figure 3). These wavelengths agreed with the absorption maxima of the oxygen adduct and the deoxy complex in Figure 1. The validity of this measurement is supported further by the following results: (1) Absorbance at 538 nm is constant before and after flash photolysis (Figure 3). This wavelength agrees with the isosbestic point of the oxygen adduct and the deoxy complex as shown in Figure 1. (2) The absorption changes followed at 528 and 545 nm are symmetric (Figure 3).

The k_{on} and k_{off} were estimated by pseudo-first-order kinetics (Figure 3) and are given in Table I. The k_{on} and k_{off} values of the CoPIm complex in the membrane were a little faster than or similar to those of the complex in toluene solution. This means that the CoPIm complex is active for oxygen binding even in the membrane and acts as an effective fixed carrier of oxygen.

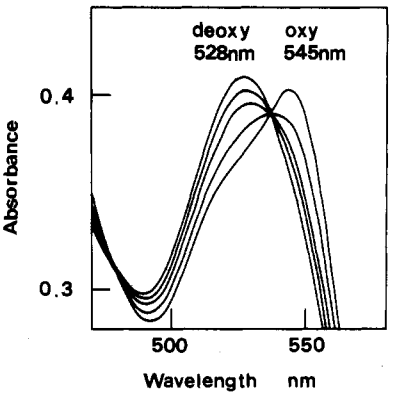

Figure 1. Visible absorption spectral change in the oxygen binding to the CoPIm/PBMA membrane at 25 °C, [CoPIm] = 2.5 wt %.

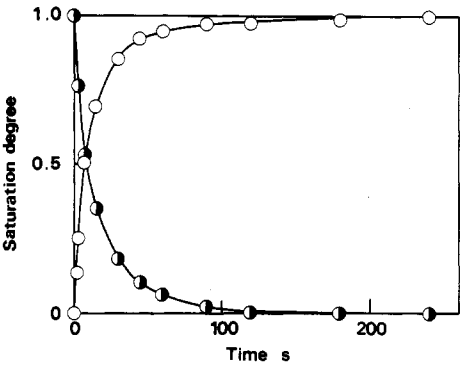

Figure 2. Time course of the oxygen adsorption (○) and desorption (◑) in the CoPIm/PBMA membrane at 25 °C, [CoPIm] = 2.5 wt %.

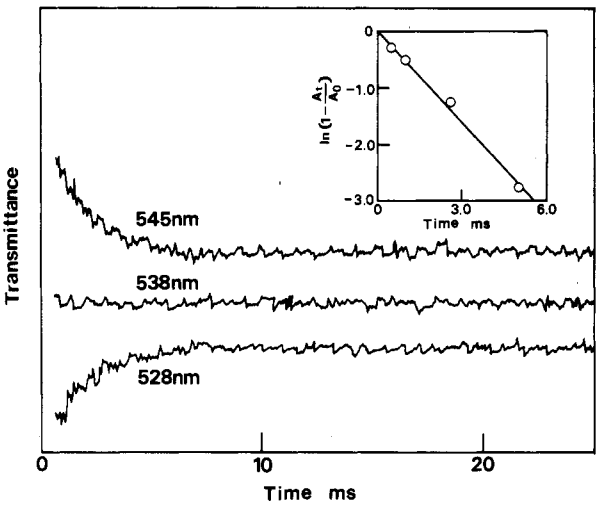

Figure 3. Flash photolysis of the CoPIm/PBMA membrane under exposure to air and approximation to pseudo-first-order kinetics for the membrane at 25 °C, [CoPIm] = 2.5 wt %.

Table I
Oxygen-Binding Rate, Equilibrium Constants,[a] and Thermodynamic Parameters[b] for the CoPIm/PBMA Membrane

physical state	$10^{-5}k_{on}$, L mol^{-1} s^{-1}	$10^{-4}k_{off}$, s^{-1}	K, L mol^{-1}	ΔH, kcal mol^{-1}	ΔS, eu
toluene soln	1.2	1.2	10.1	−12	−36
membrane	5.2	2.8	18.6	−14	−44

[a] Data at 25 °C. [b] Data from Figure 5 (ln K in atm^{-1}).

The oxygen-binding equilibrium constant ($K = k_{on}/k_{off}$) was determined from the oxygen-binding and dissociation equilibrium measurement by using Drago's equation.[11] The oxygen-binding equilibrium curves are given in Figure

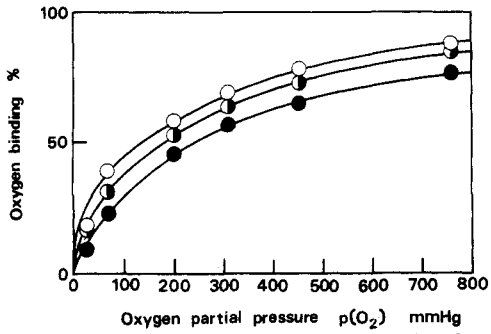

Figure 4. Oxygen-binding equilibrium curve for the CoPIm/PBMA membrane at (○) 20 °C, (◑) 25 °C, and (●) 30 °C. [CoPIm] = 2.5 wt %.

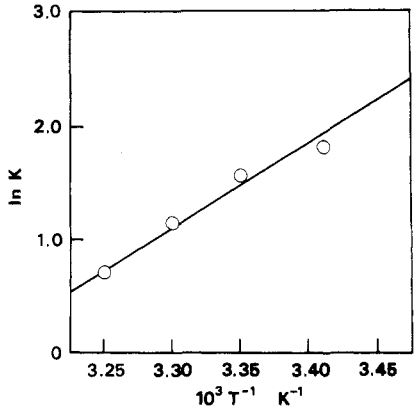

Figure 5. van't Hoff plots of the oxygen-binding equilibrium constants for the CoPIm/PBMA membrane, [CoPIm] = 2.5 wt %.

4. The K ($mmHg^{-1}$) obtained was converted to K (M^{-1}) by substituting the solubility coefficient of oxygen in the membrane determined by the oxygen permeation measurement mentioned later (Table I). The K value of the complex in the membrane was a little larger than or similar to that in the toluene solution.

The thermodynamic parameters for oxygen binding were estimated from the temperature dependence of K (Figure 5) and are also given in Table I. The enthalpy change (ΔH) for the complex in the membrane is more negative than that for the solution. This favorable enthalpy change contributes to the slightly larger K values of the membrane system. The larger oxygen-binding affinity of the CoPIm complex fixed in the membrane in comparison with that in the solution may be explained as follows. While the axial Im ligation is at equilibrium in the solution system, the CoP–Im complexation is completed and/or the Im ligand is immobilized to CoP, which brings about relatively stable oxygen adduct formation for the complex in the membrane.

The advantages of the membrane containing CoPIm are that the fixed carrier maintains its rapid and reversible binding capability of the penetrant even after fixation in the membrane and that adsorption and desorption rate and equilibrium constants of the penetrant at the carrier site can be evaluated in situ.

Oxygen Permeability in the Fixed Carrier Membrane. Figure 6 shows the effect of upstream gas pressure (p_2) on the permeability coefficients (P_{O_2} and P_{N_2}) in the membrane containing 2.5 wt % CoPIm. P_{O_2} increases with the decrease in $p_2(O_2)$, which is in accordance with eq 1. Although the dependence of P on p_2 has often been reported for glassy polymers,[9] glass transition temperatures were 19, 15, and 20 °C for the membranes containing 0, 2.5, and 4.5 wt % CoPIm, respectively, and the membranes

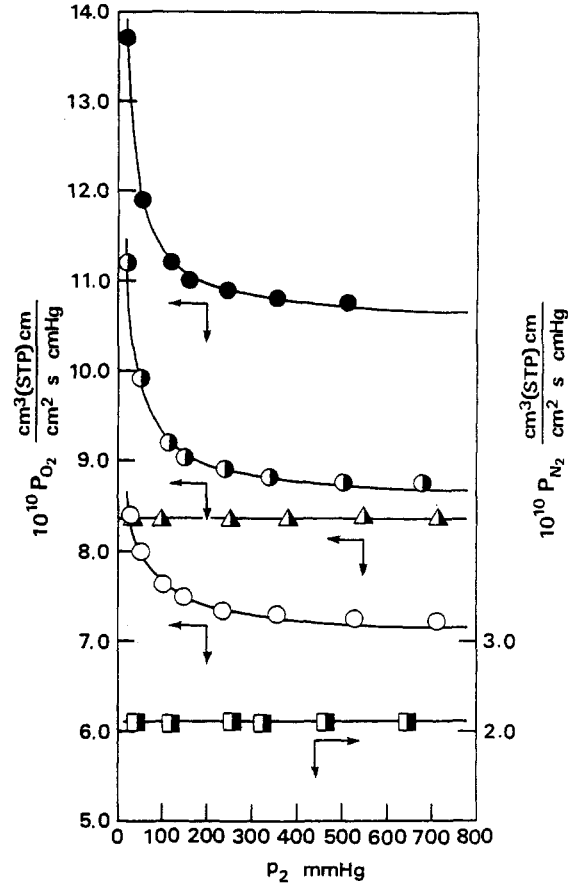

Figure 6. Effect of upstream gas pressure on permeation coefficient for the CoPIm/PBMA membrane (oxygen at (○) 20 °C, (◑) 25 °C, (●) 30 °C; nitrogen at (◨) 25 °C) and for the inert CoPIm/PBMA membrane (oxygen at (▲) 25 °C).

were in a rubbery state at the temperatures employed for the permeability measurements. In fact, P_{N_2} was independent of $p_2(N_2)$ because the fixed carrier does not interact with nitrogen. This was also supported by the fact that P_{O_2} was independent of $p_2(O_2)$ for a membrane containing the inert cobalt(III) complex (2.5 wt %), which does not interact with or bind oxygen.

The induction period (θ) for oxygen permeation also depended on $p_2(O_2)$ in the same manner as the permeation coefficient, as shown in Figure 7. This behavior is in agreement with eq 2 and indicates that oxygen clearly interacts with the CoPIm complex in the membrane. This is further supported by the results that θ for nitrogen permeation in the membrane containing the carrier and θ for oxygen permeation in the membrane containing the inert complex are independent of the upstream gas pressures. In Figure 7 one also notices that θ_{O_2} and the $p_2(O_2)$ dependence of θ_{O_2} decrease with temperature. θ_{O_2} and the $p_2(O_2)$ dependence of θ_{O_2} are based on oxygen binding to the fixed carrier and enhanced at lower temperature because the oxygen-binding equilibrium constant of the fixed carrier increases with decreasing temperature (see Table I).

The effect of $p_2(O_2)$ on P_{O_2} was analyzed by using eq 1; that is, P_{O_2} was plotted against $1/(1 + Kp_2)$ (Figure 8). The plots show a linear relationship: the oxygen permeability in the membrane containing the complex as a fixed carrier can be explained in terms of the sum of the Henry mode attributed to the matrix and the Langmuir mode attributed to the fixed carrier, that is, a dual-mode model.

The effect of $p_2(O_2)$ on the induction period was analyzed by using eq 3. The FR value calculated from the

Table II
Dual-Mode Transport Parameters for the CoPIm/PBMA Membrane

T, °C	D_D, cm^2 s^{-1}	D_C, cm^2 s^{-1}	F (D_C/D_D)	k_D, cm^3 (STP) cm^{-3} cmHg^{-1}	C_C', cm^3 (STP) cm^{-3}	K, cmHg^{-1}
20	6.6×10^{-7}	1.2×10^{-8}	0.02	1.1×10^{-3}	0.2	8.4×10^{-2}
25	7.0×10^{-7}	1.4×10^{-8}	0.02	1.0×10^{-3}	0.2	5.6×10^{-2}
30	1.1×10^{-6}	2.0×10^{-8}	0.02	9.2×10^{-4}	0.2	3.8×10^{-2}

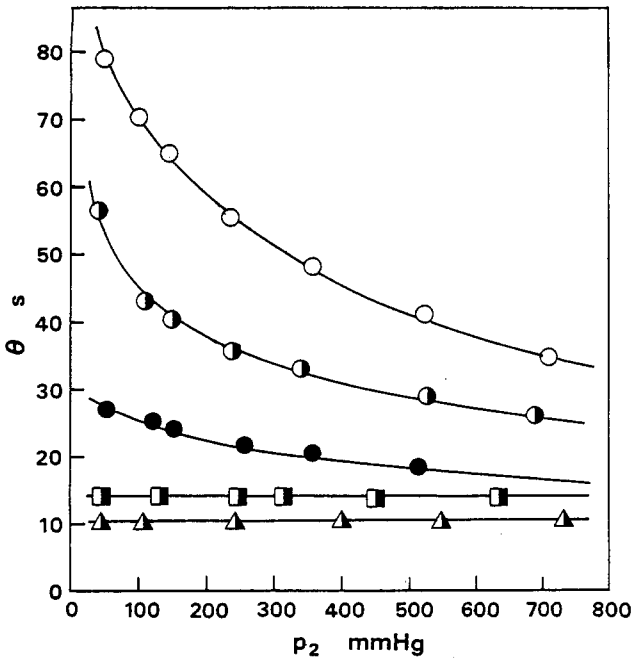

Figure 7. Effect of upstream gas pressure on induction period for the CoPIm/PBMA membrane (oxygen at (○) 20 °C, (◑) 25 °C, and (●) 30 °C; nitrogen at (◨) 25 °C) and for the inert CoPIm/PBMA membrane (oxygen at (▲) 25 °C).

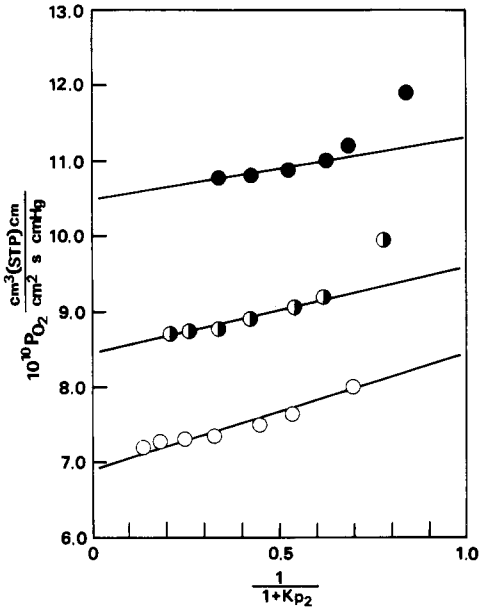

Figure 8. Oxygen permeability in the CoPIm/PBMA membrane plotted according to eq 1 (at (○) 20 °C, (◑) 25 °C, and (●) 30 °C).

slope and intercept of the linear relationship in Figure 8 was substituted in eq 3; the left-hand term (Y) was plotted against the right-hand term (X) (Figure 9), also giving a linear relationship, which also supports the dual-mode transport of oxygen in the membrane and a pathway of oxygen permeation via the fixed carrier.

D_D and R ($C_C'K/k_D$) were calculated from the slope and intercept of the linear relationship in Figure 9, and F (= D_C/D_D) was given from FR (Table II). The results show that Langmuir-sorbed oxygen has ca. 2% of the mobility of that due to the Henry mode.

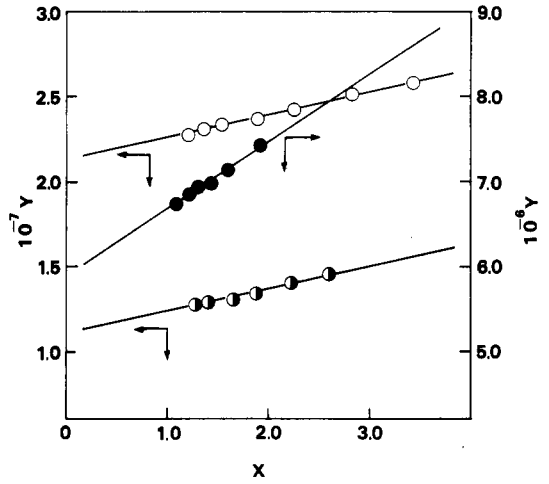

Figure 9. Oxygen permeability parameters in the CoPIm/PBMA membrane plotted according to eq 3 (at (○) 20 °C, (◑) 25 °C, (●) 30 °C).

Table III
Oxygen Permeability Coefficient (at 25 °C) and Permeability Ratio (P_{O_2}/P_{N_2})

CoPIm in membrane, wt %	permeability coeff[a]	P_{O_2}/P_{N_2}
0	6.4	3.2
2.5	12	5.7
4.5	23	12

[a] Upstream pressure: 5.0 mmHg. The permeability coefficient is expressed in units of (cm^3 (STP) cm/(cm^2 s cmHg)) × 10^{10}.

Although dual-mode transport due to partial immobilization[9] has been reported for carbon dioxide permeation in glassy polymers, we have verified the dual-mode transport using a much simpler system.

The effect of the fixed carrier concentration in the membrane on the permselectivity is shown in Table III. The permeability ratio (P_{O_2}/P_{N_2}) was above 10 for the membrane containing 4.5 wt % CoPIm complex at the upstream pressure of 5.0 mmHg. This result indicates the possibility of high permselectivity with a membrane containing a fixed carrier. High permselectivity for the membrane containing a much larger amount of the CoPIm complex will be reported in a subsequent paper.

Acknowledgment. This work was partially supported by a Grant-in-Aid from the Ministry of Education, Science, and Culture, Japan.

Registry No. CoPIm, 53675-32-4; PBMA, 9003-63-8; O_2, 7782-44-7.

References and Notes

(1) Gardner, R. J.; Crane, R. A.; Hannan, J. F. *Chem. Eng. Prog.* **1977**, *10*, 73.
(2) Comyn, J., Ed. *Polymer Permeability*; Elsevier: New York, 1985.
(3) Kesting, R. E. *Synthetic Polymeric Membrane*, 2nd ed.; McGraw-Hill: New York, 1985.

(4) (a) Tsuchida, E. *J. Macromol. Sci., Chem.* **1979**, *A13*, 545. (b) Tsuchida, E.; Nishide, H.; Yuasa, M.; Hasegawa, E.; Matsushita, Y.; Eshima, K. *J. Chem. Soc., Dalton Trans.* **1985**, 275. (c) Tsuchida, E. *Ann. N.Y. Acad. Sci.* **1985**, *446*, 429. (d) Tsuchida, E. *Chem. Eng. News* **1985**, *63*(2), 42.
(5) (a) Koval, C. A.; Noble, R. D.; Way, J. D.; Lovie, B.; Reyes, Z. E.; Batman, B. R.; Horn, G. M.; Reed, D. L. *Inorg. Chem.* **1985**, *24*, 1147. (b) Roman, I. C.; Baker, I. W. U.S. Patent 4 542 010, 1985.
(6) Nishide, H.; Ohyanagi, M.; Okada, O.; Tsuchida, E. *Macromolecules* **1986**, *19*, 495.
(7) (a) Nishide, H.; Kuwahara, M.; Ohyanagi, M.; Funada, Y.; Kawakami, H.; Tsuchida, E. *Chem. Lett.* **1986**, 43. (b) Drago, R. S.; Balkus, K. J. *Inorg. Chem.* **1986**, *25*, 716. (c) Nishide, H.; Ohyanagi, M.; Kawakami, H.; Tsuchida, E. *Bull. Chem. Soc. Jpn.* **1986**, *59*, 3213.
(8) Collman, J. P.; Brauman, J. I.; Coxsee, K. M.; Halbert, T. R.; Hayes, S. E.; Suslick, K. S. *J. Am. Chem. Soc.* **1978**, *100*, 2761.
(9) (a) Paul, D. R.; Koros, W. J. *J. Polym. Sci., Polym. Phys. Ed.* **1976**, *14*, 675. (b) Paul, D. R. *Ber. Bunsen-Ges. Phys. Chem.* **1979**, *83*, 294.
(10) (a) Wohrle, D.; Bohlen, H.; Aringer, C. *Makromol. Chem.* **1984**, *185*, 669. (b) Tsuchida, E.; Honda, K.; Hata, S. *Bull. Chem. Soc. Jpn.* **1976**, *49*, 868.
(11) Beugelsdijk, T.; Drago, R. S. *J. Am. Chem. Soc.* **1975**, *97*, 6466.

Relaxation Behavior of the β Phase of Poly(butylene terephthalate)

B. C. Perry, J. L. Koenig,* and J. B. Lando

Department of Macromolecular Science, Case Western Reserve University, Cleveland, Ohio 44106. *Received June 30, 1986*

ABSTRACT: Poly(butylene terephthalate) undergoes a unique reversible crystalline α to β phase transition when uniaxially drawn. The strained (β) phase of poly(butylene terephthalate) was obtained in a metastable form by cold-drawing a fiber sample approximately 250% (>50% crystallinity). Wide-angle X-ray diffraction, diffuse-reflectance IR, and ^{13}C CP-MAS-DD experiments confirm the presence of the β phase. ^{13}C relaxation measurements involving spin-lattice relaxation in the rotating frame, $T_{1\rho}$, indicate that the aromatic rings in the β phase possess more molecular motion than those in the α phase. Spin-lattice relaxation measurements, T_1, indicate that the terephthalate residue has increased mobility with respect to the α phase, which indicates the driving force behind the reversible crystal-crystal transition is indeed the packing efficiency of the aromatic rings in the α phase. The interior methylenes have motions of greater frequency and or amplitude with respect to the exterior methylenes in both phases.

Introduction

^{13}C NMR spectroscopy is an analytical tool that not only probes static structural information but also allows dynamic measurements over a broad frequency range. The available frequency range is from the kilohertz region (^{13}C $T_{1\rho}$) to the megahertz region (^{13}C T_1). The relaxation behavior of the α-crystalline phase of poly(butylene terephthalate) (PBT) (Figure 1) has been studied extensively by Jelinski et al.[1-10] The β-crystalline phase in PBT has not been studied to date by ^{13}C NMR.

PBT is a unique polymer because it undergoes a reversible crystal-crystal phase transition when uniaxially stretched. It has been clearly shown by IR and WAXS[11-26] that the α (relaxed) to β (strained) transition occurs at strains as low as 5% and that the transition is complete at 15% strain. When tension is released, the polymer reverts rapidly back to the α phase with little hysteresis. Static measurements have shown the major differences between the phases lies in the conformation of the tetramethylene segments. The α phase is A-T-A (where A = non-trans, non-gauche and T = trans) and the β phase is the extended T-T-T configuration. It is believed that the driving force behind the reversible transition is the enhanced packing efficiency of the terephthalate groups in the α phase.

In the past, constant tension was required to maintain a stable β phase. The restraint of constant tension precluded magic-angle spinning NMR experiments. This problem has been avoided by using a fiber sample obtained from Celanese Corp. The fiber, as spun, is an oriented, semicrystalline sample with the α phase being the dominant form. Cold-drawing the fibers approximately 250% and releasing the tension create an oriented "metastable" β phase for which magic-angle spinning (MAS) experiments can be performed. Infrared studies of the β-phase fibers before and after the MAS NMR experiment show negligible change in the amount of β phase.

In this paper, MAS-CP-DD experiments are reported on this "metastable" β phase. In addition, T_1 and $T_{1\rho}$ measurements are reported for both phases.

Experimental Section

A commercially prepared melt-spun semicrystalline PBT fiber sample was obtained from Celanese Corp. The unstretched fibers refer to the samples as received. Drawn fibers are obtained by cold-drawing on a stretch rack at room temperature to a strain of approximately 250%. Annealed samples are obtained by heating the fibers at 200 °C for approximately 8 h in vacuo with no tension.

Diffuse-reflectance (DRIFT) IR spectra are obtained on a FTS-20 Digilab FTIR spectrophotometer equipped with a narrow band-pass mercury cadmium telluride (MCT) detector. All spectra are recorded in the absorbance mode with double precision at a resolution of 2 cm^{-1}. Two hundred scans of both sample and KBr reference are collected to obtain a better S/N ratio. All spectra are transferred to a DEC VAX 11/780 computer operating under VMS 3.7 for data processing. The reflectance spectra are plotted according to the Kubelka-Monk algorithm.

Wide-angle X-ray diffraction patterns are obtained with a Statton camera (nickel-filtered Cu Kα radiation, λ = 1.5418 Å). Sample-to-film distance is calibrated with CaF_2 powder. The exposure time for each sample varied, depending on the degree of crystallinity and sample-to-film distance.

^{13}C NMR spectra are recorded at 37.7 MHz on a modified Nicolet NT-150 spectrometer. Magic-angle spinning,[27] cross polarization[28] and dipolar decoupling[29] are used simultaneously for the CP experiments. The radio-frequency fields are typically

0024-9297/87/2220-0422$01.50/0